Electronic Supplementary Material (ESI) for Journal of Materials Chemistry A.

Supporting Information

High-performance $NaFePO_4$ formed by Aqueous Ion-exchange and its mechanism for advanced Sodium Ion Batteries

Wei Tang[a,f,g,+], Xiaohe Song[b,+], Yonghua Du[c,+], Chengxin Peng[a,g], Ming Lin[d], Shibo Xi[c], Bingbing Tian[a,g], Jiaxin Zheng[b], Yuping Wu[e], Feng Pan[b,*], Kian Ping Loh [a,g,*]

[a]Department of Chemistry, National University of Singapore, 3 Science Drive 3, Singapore 117543.
[b]School of Advanced Materials, Peking University Shenzhen Graduate School, Shenzhen, China, 518055.
[c]Institute of Chemical and Engineering Sciences, A*STAR, 1 Pesek Road, Jurong Island, Singapore, 627833.
[d]Institute of Materials Research and Engineering, 2 Fusionopolis Way, #08-03 Innovis, Singapore 138634.
[e]New Energy and Materials Laboratory (NEML), Department of Chemistry & Shanghai Key Laboratory of Molecular Catalysis and Innovative Materials, Fudan University, Shanghai, China, 200433.
[f]NUS Graduate School for Integrative Sciences and Engineering, 28 Medical Drive #05-01, Singapore 117597.
[g]Centre for Advanced 2D Materials and Graphene Research Centre, National University of Singapore, 6 Science Drive 2, Singapore 117546

*Corresponding Author
Kian Ping Loh, Email: chmlohkp@nus.edu.sg; Feng Pan, Email: panfeng@pkusz.edu.cn

+These authors contributed equally

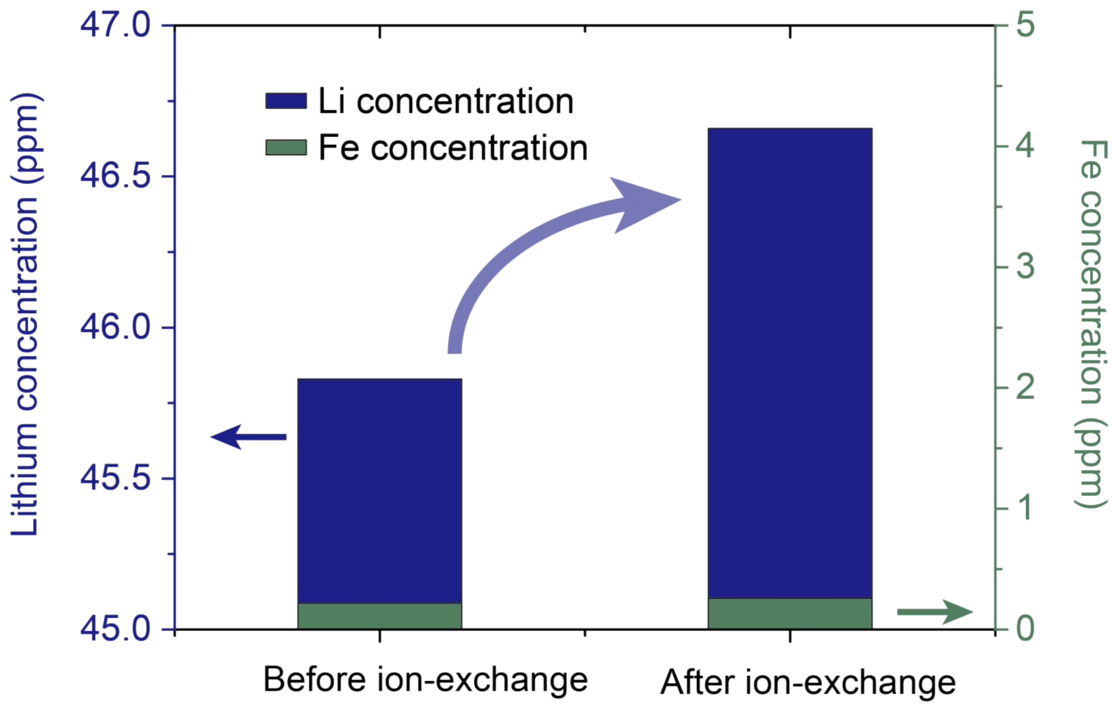

Figure S1. Li ions and Fe ions concentrations in the aqueous electrolyte before and after ion-exchange process.

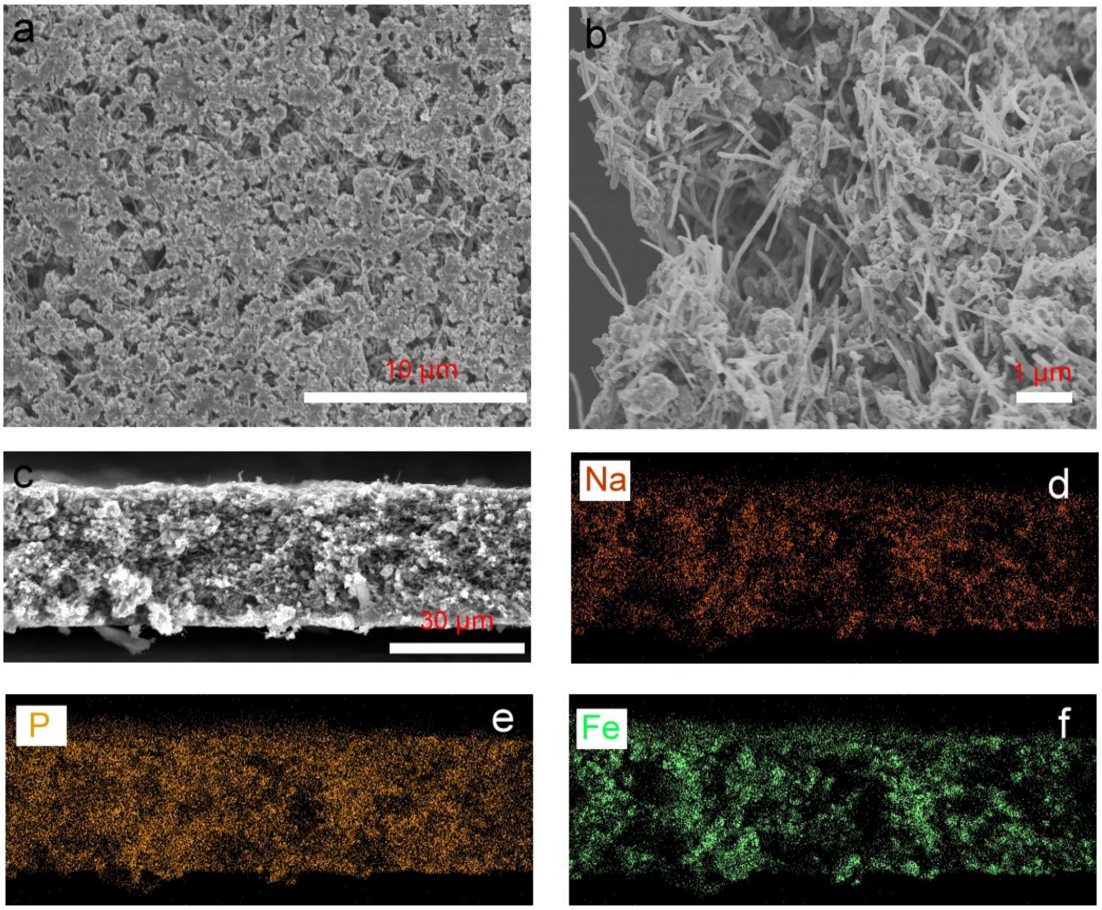

Figure S2 (a),(b) SEM images of $NaFePO_4$ eletrodes obtained from aqueous ion-exchange; (c) SEM image of the cross section of $NaFePO_4$ eletrodes obtained from aqueous ion-exchange and corresponding EDX mapping of (d) Na, (e) P and (f) Fe.

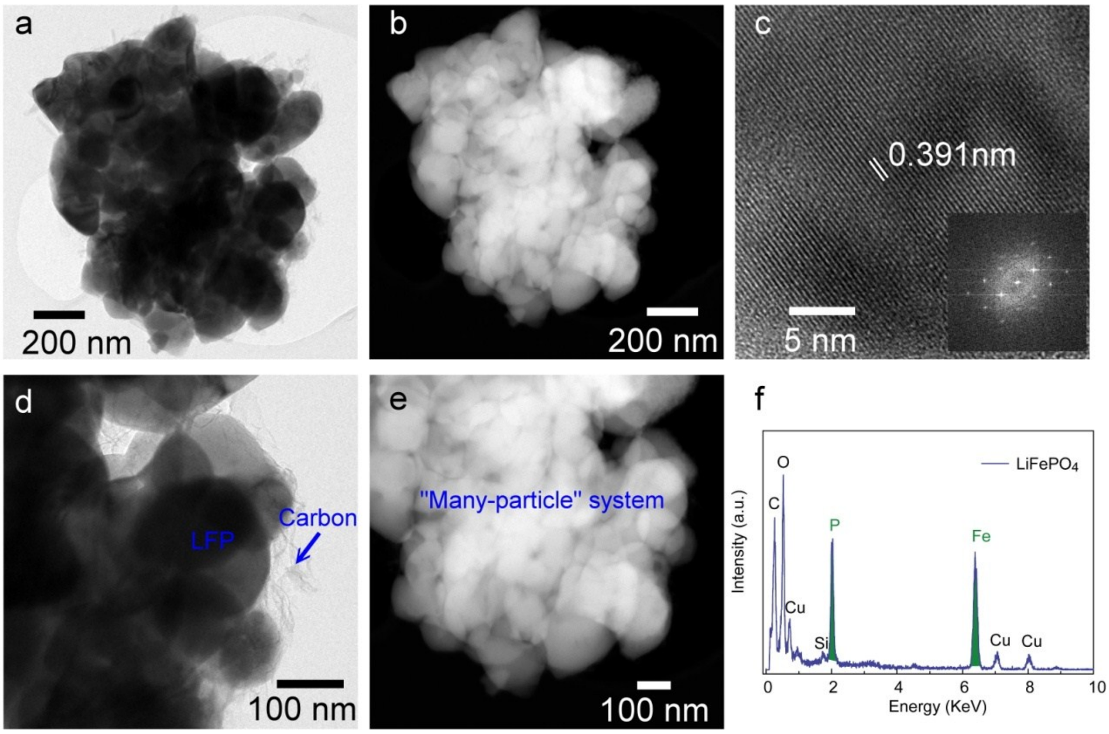

Figure S3. Characterizations of the pristine $LiFePO_4$. (a),(d) TEM images;(b),(e) STEM images; (c) High resolution TEM image to show lattice fringe of $LiFePO_4$; (f) EDX analysis of $LiFePO_4$. As clearly shown in (d) and (e), the pristine $LiFePO_4$ consist of many particles coated with a thin layer carbon.

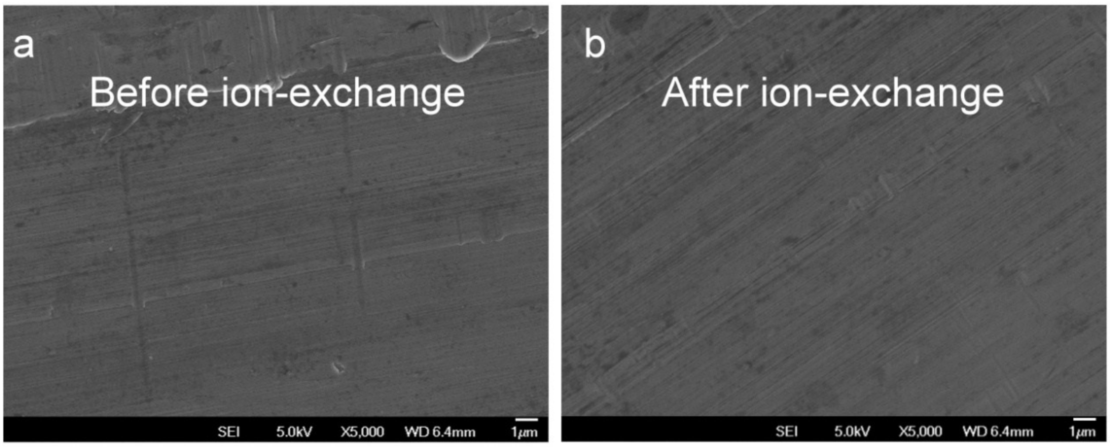

Figure S4. SEM images of Aluminum foil (current collector) (a) before and (b) after aqueous ion-exchange.

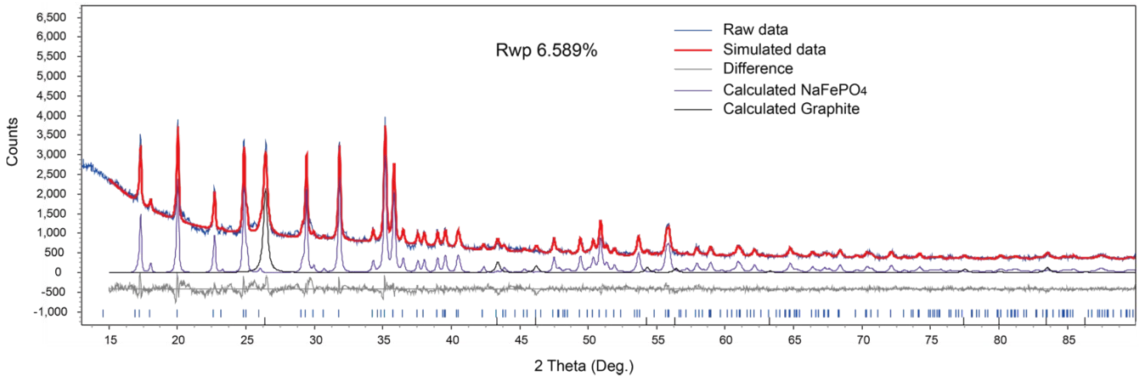

Figure S5. Rietveld refinement result for the XRD diffraction patterns of the $NaFePO_4$ by aqueous ion-exchange.

Table S1. Refined lattice parameters of the $NaFePO_4$ by aqueous ion-exchange

Parameters	a	b	c
$NaFePO_4$	10.2898 (9)	6.0838 (5)	4.9319 (5)

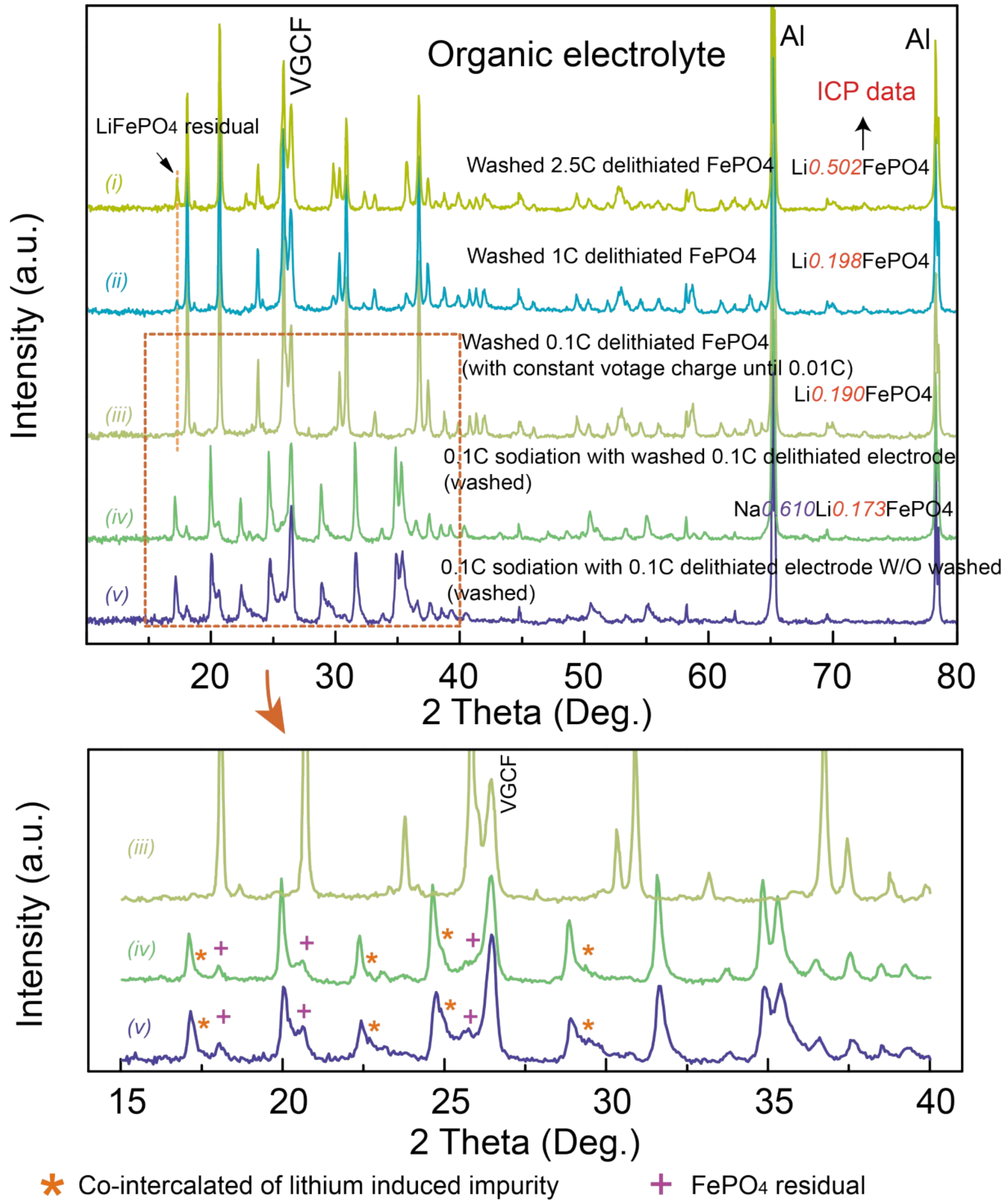

Figure S6. XRD patterns / ICP analysis of delithiated $FePO_4$ electrodes and as-prepared $NaFePO_4$ electrodes based on organic ion-exchange.

As shown in Figure S6, the residual Li^+ shown in ICP analysis should be contributed to two sources: 1) un-delithiated $LiFePO_4$ due to reaction dynamic, 2) Li^+ absorbed on the surface of materials. By applying a slower delithiated rate (ii) and constant voltage charge (iii), the un-lithiated contribution should be neglectable (as shown in the XRD patterns), while the residual Li^+ should be mainly contributed to the surface adsorption. Upon sodiation, the adsorption Li^+ may co-intercalate into the carefully washed $FePO_4$ host, inducing the impurity of $NaFePO_4$ as indicated in enlarged pattern (iv) as "*"; moreover, the residual of $FePO_4$ after sodiation has also been indicated in the pattern as "+". Sodiated with delithiated $FePO_4$ without washing, there is a large amount of Li^+ adsorbed on the surface, which may result more Li-co-intercalation (v).

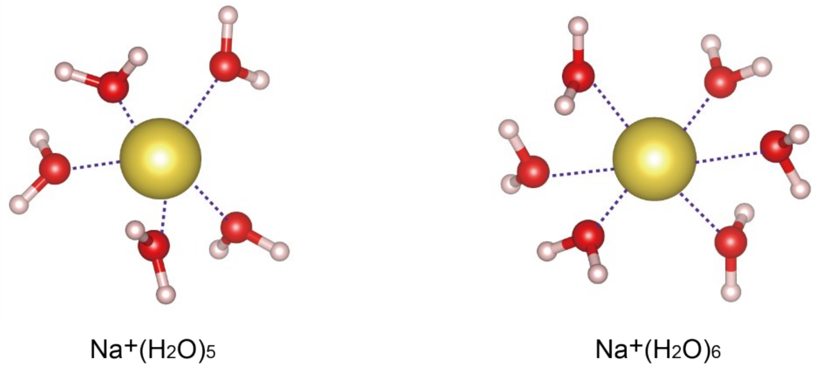

Figure S7. Illustration of the structures of $Na^+(H_2O)_5$ and $Na^+(H_2O)_6$ complexes.

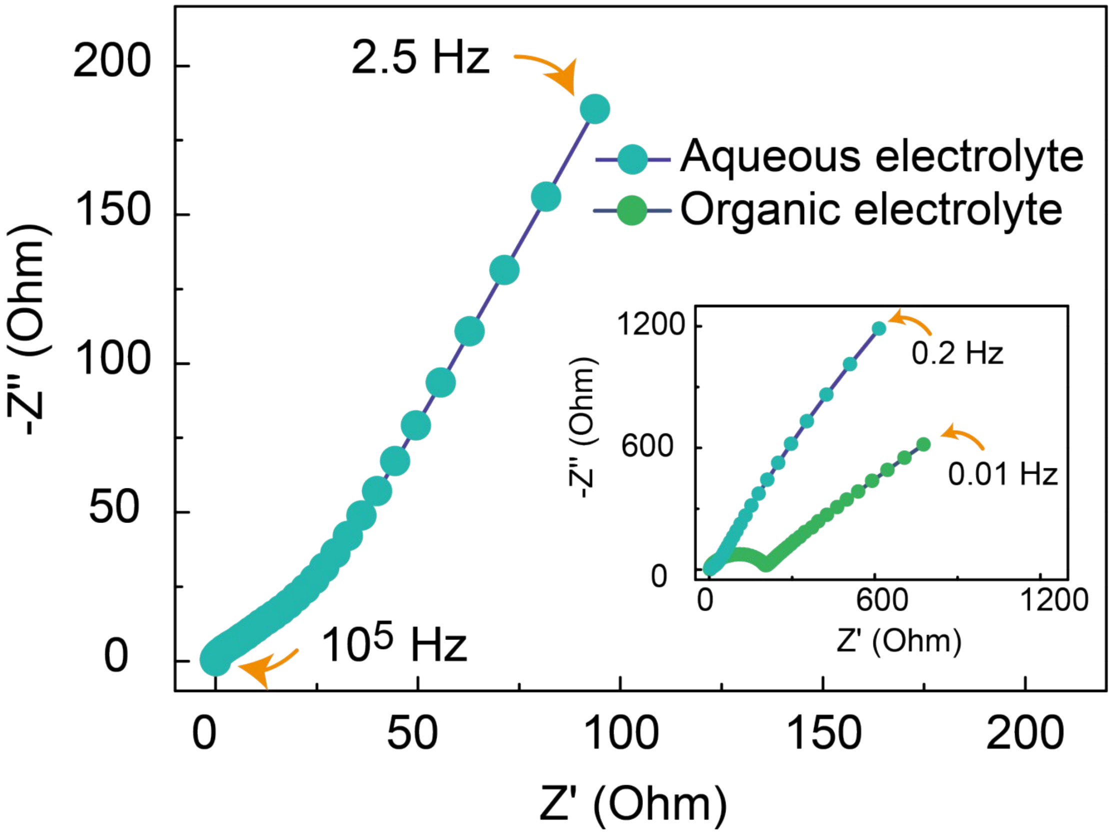

Figure S8. Nyquist plots of $LiFePO_4$ electrodes in aqueous and organic electrolytes.

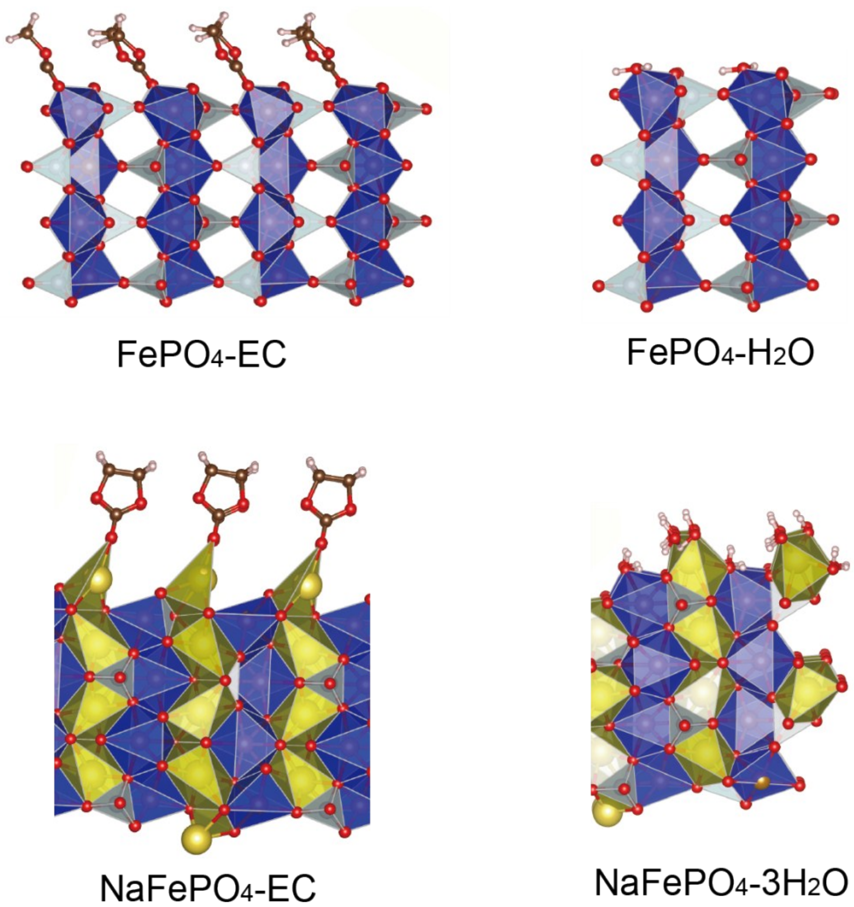

Figure S9. *Ab* initio calaculated H_2O/EC adsorption at $FePO_4$ and $NaFePO_4$.

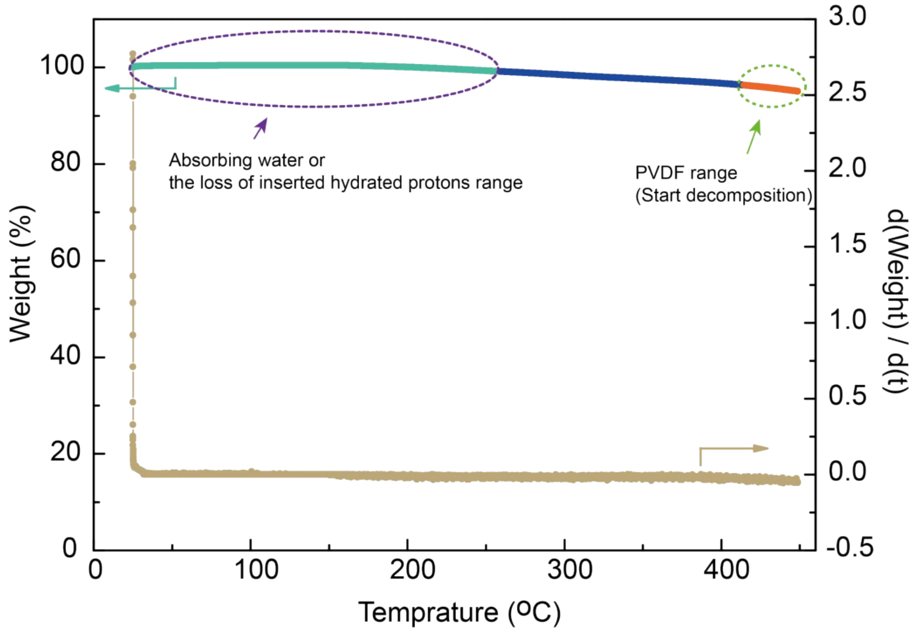

Figure S10. TGA plot of $NaFePO_4$ obtained by aqueous ion-exchange dried at 80ºC.

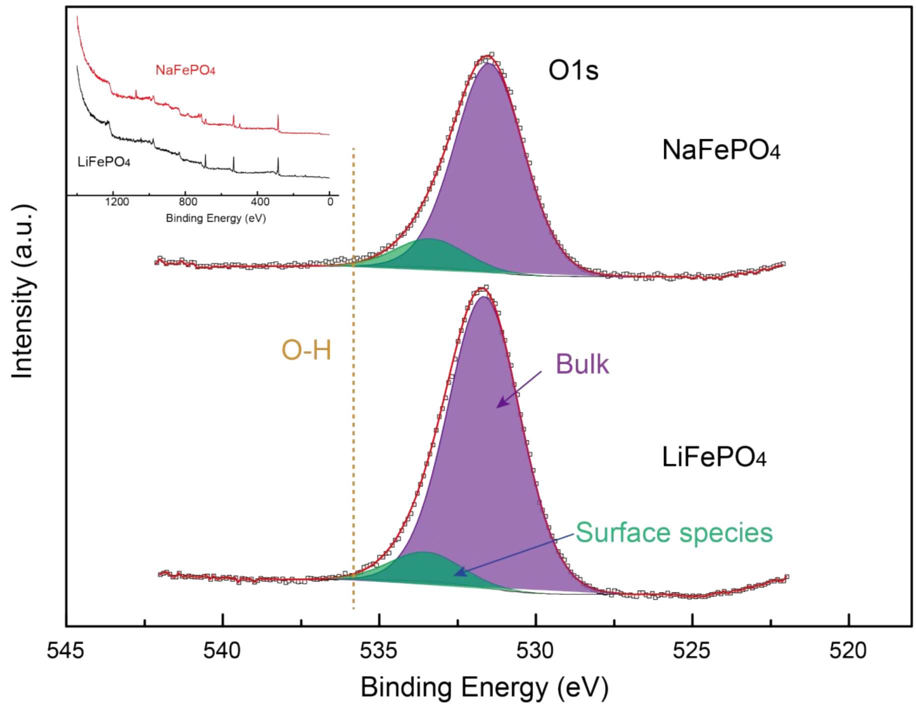

Figure S11. O^{1s} XPS spectra of the $NaFePO_4$ obtained from aqueous-exchange and pristine $LiFePO_4$ eletrodes.

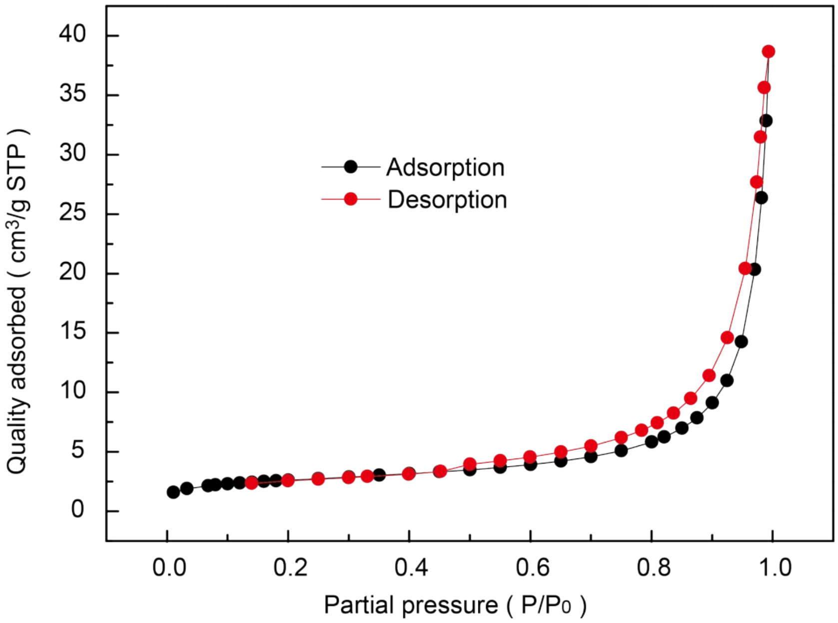

Figure S12. BET isotherms of the $NaFePO_4$ obtaiend from aqueous ion-exchange to reveal the specific surface area.

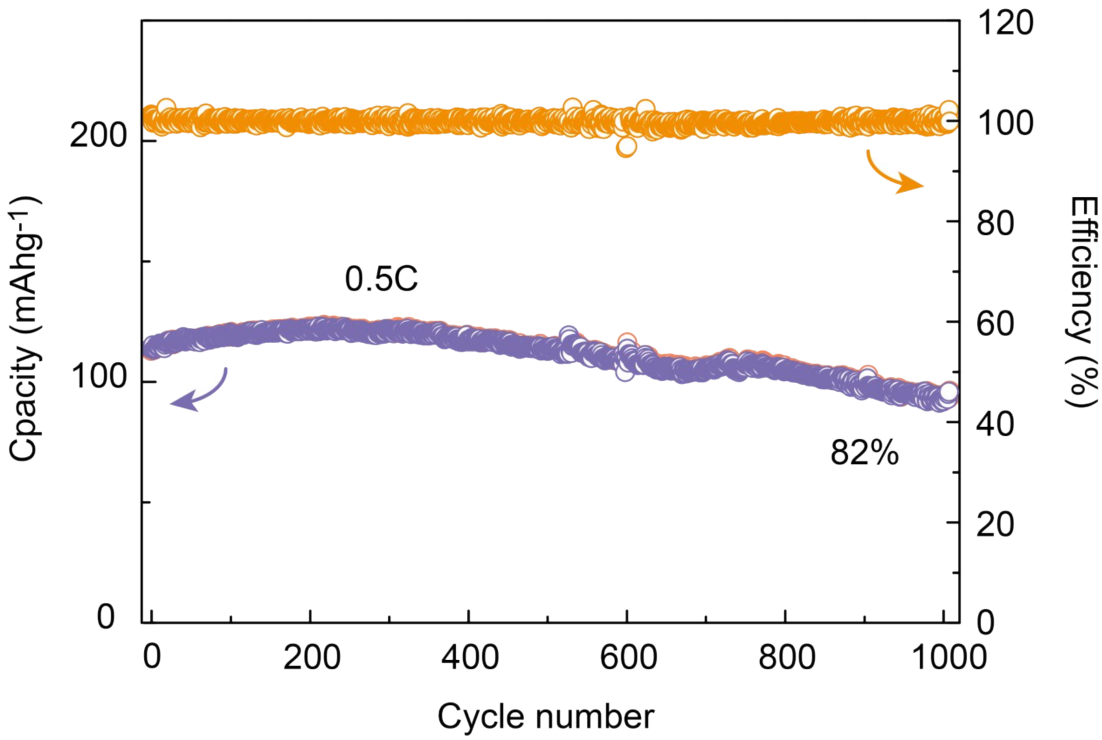

Figure S13. Long-term cycles of aqueous ion-exchanged $NaFePO_4$ up to 1000 cycles at 0.5C.

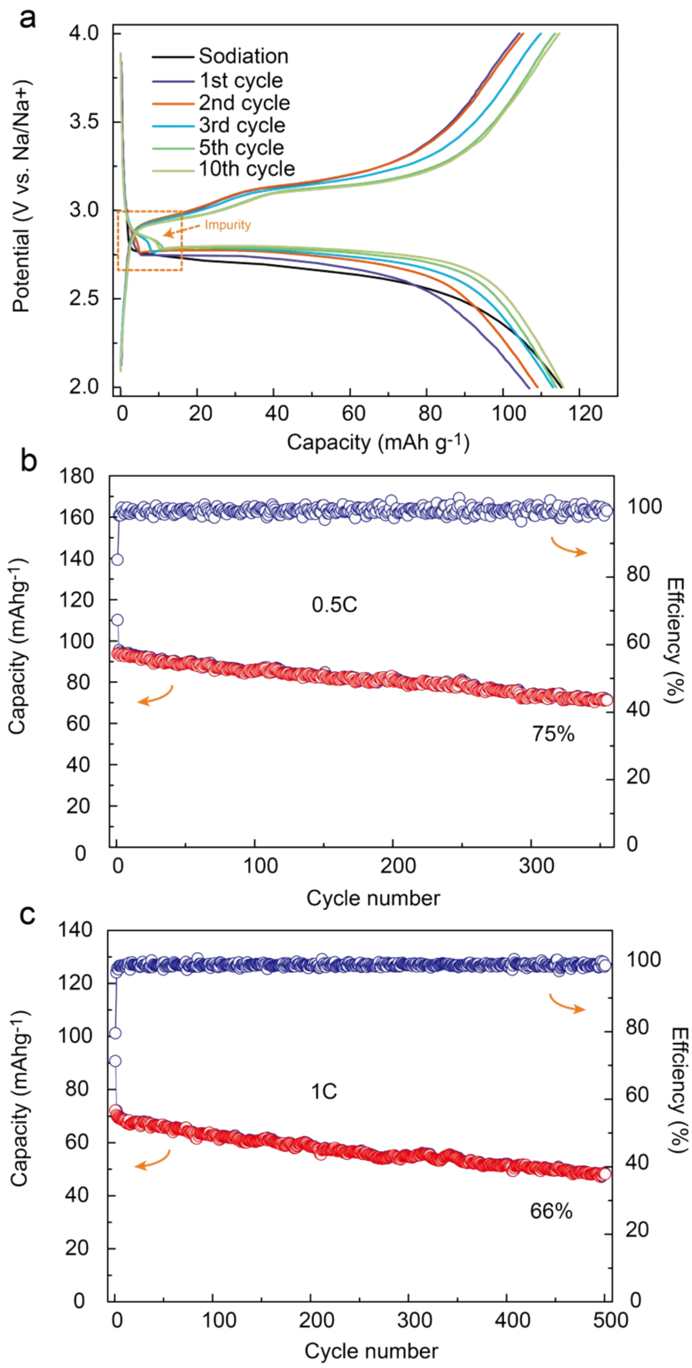

Figure S14. Electrochemical performance of $NaFePO_4$ driven from organic ion-exchange.

As shown in Figure S14a, a set of additional plateaus were observed at the discharge process (marked as box), which may be due to the impurity of Lithium insertion. The same phenomena have been previous observed by Bruno Scrosati, Yang-Kook Sun at al.[1]

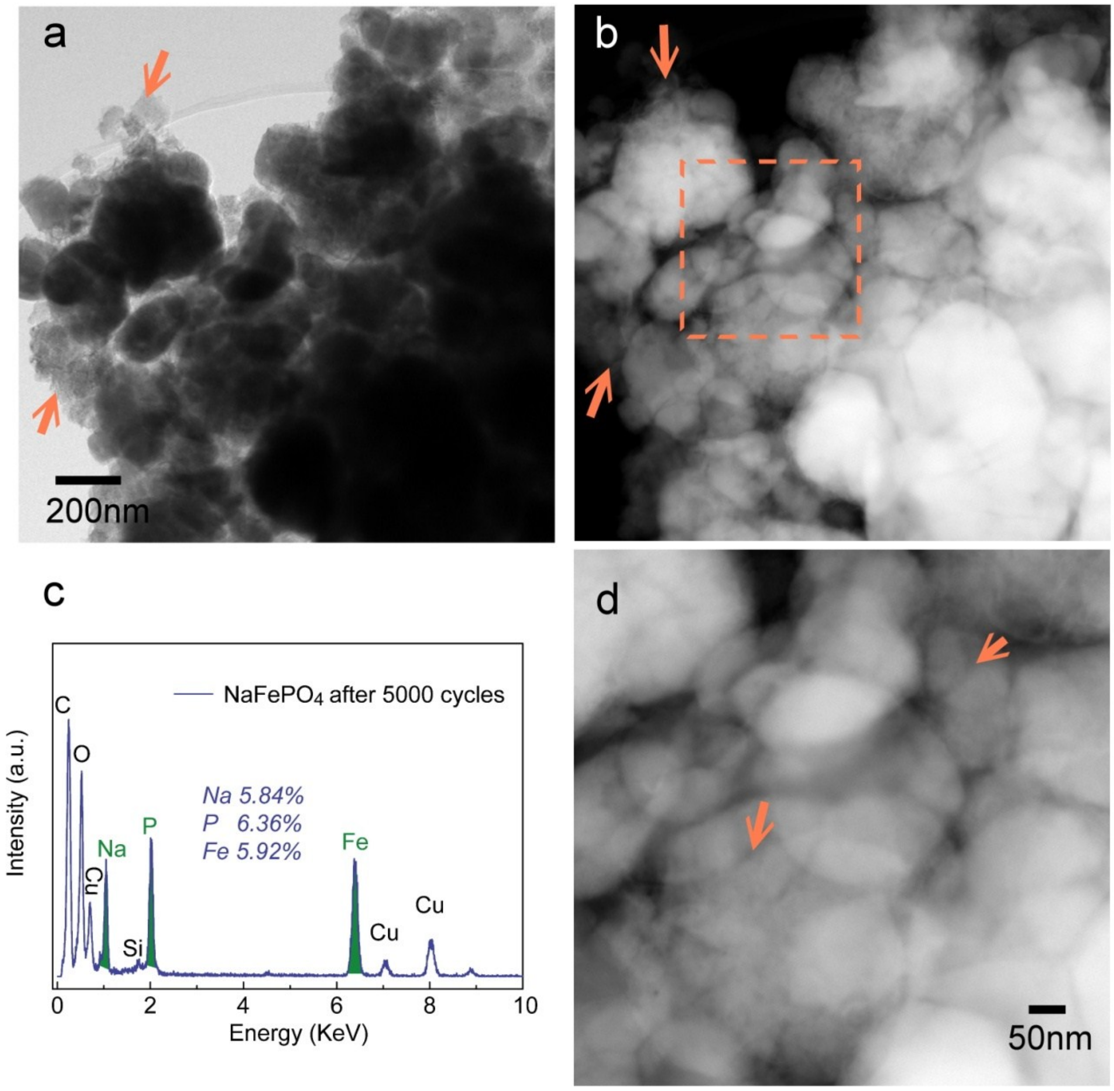

Figure S15. Characterization of $NaFePO_4$ driven from aqueous ion-exchange after 5000 cycles. (a) TEM and (b),(c) STEM images to demonstrate the small amount crack of $NaFePO_4$ electrodes after 5000 cycles, according to the minor boarding of XRD peaks after 5000 cycles. (c) EDX analysis of $NaFePO_4$ electrodes after 5000 cycles.

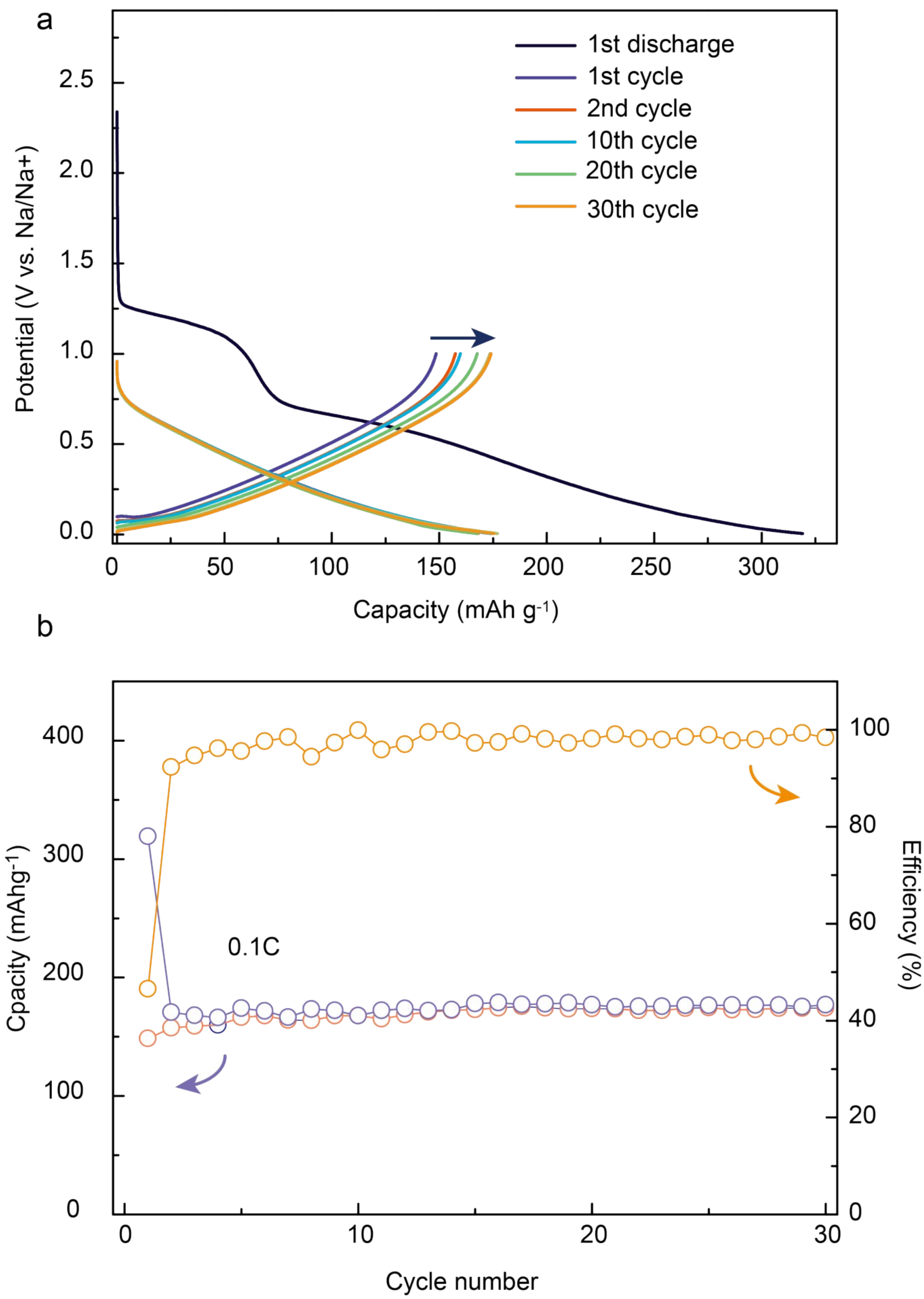

Figure S16. (a) Voltage profile and (b) cyclibility of hard carbon at 0.1C. As shown in (a) the charge and discharge plot of commercial hard carbon is sloping plot without obvious plateau. That should be associated with the sloping voltage profile of $NaFePO_4$ // hard carbon full cell.

Supporting section 1: The desolvation and adsorption process for extracting M-ion (M=Li, Na) from solvated M-ion in electrolytes to $FePO_4$ surface.

1.1 The desolvation process

The desolvation process for hydrated M-ion in aqueous solution is described as:

$$M^+(H_2O)_n\ (aq) \rightarrow M^+(H_2O)_{n-1}\ (aq) + H_2O\ (aq) \quad (1)$$

The successive detaching energy in Equation 13 is defined as:

$$\Delta E_{n,n-1\_H2O}=E[M^+(H_2O)_n]_{aq}-E[M^+(H_2O)_{n-1}]_{aq}-E(H_2O)_{aq} \quad (2)$$

where $E[M^+(H_2O)_n]_{aq}$, $E[M^+(H_2O)_{n-1}]_{aq}$, and $E(H_2O)_{aq}$ denote the total energies of $M^+(H_2O)_n$, $M^+(H_2O)_{n-1}$, and H_2O in the experimental electrolytes, respectively.

Because the energy difference related to H_2O between the aqueous and the isolate state could be canceled out in equation 2, the above equation could express as the following equation:

$$\Delta E_{n,n-1\_H2O}=E[M^+(H_2O)_n]_{iso}-E[M^+(H_2O)_{n-1}]_{iso}-E(H_2O) \quad (3)$$

where $E[M^+(H_2O)_n]_{iso}$, $E[M^+(H_2O)_{n-1}]_{iso}$, and $E(H_2O)_{iso}$ denote the total energies of isolated $M^+(H_2O)_n$, $M^+(H_2O)_{n-1}$, and H_2O, respectively.

Previous theoretical results show that the hydrated M-ion in aqueous solution has a two-shells structure.[2, 3] The inner sphere is $Li^+(H_2O)_4$ (four H_2O molecules bonded with the Li-ion) and $Na^+(H_2O)_6$ (six H_2O molecules bonded with the Na-ion) for Li and Na, respectively. Each H_2O molecule of the second solvation shell is hydrogen-bonded to the waters of the inner shell. The detaching energy is calculated based on the system with only the inner shell ($Li^+(H_2O)_4$ and $Na^+(H_2O)_6$) because the hydrogen bonds is nontrivial comparing with $M\text{-}O_{H2O}$ bonds.

The solvated M-ion in EC electrolyte also has a two-shell structure similar to aqueous solution. The inner shell is composed of four EC forming $M^+(EC)_4$,, and the outer shell is composed of several surrounded EC molecules.[4, 5] The desolvation process and the calculation of successive detaching energy for solvated Li-ions in the organic electrolyte (EC) are similar to those for the hydrated Li-ion in aqueous electrolyte.

Since the Vienna ab initio simulation package (VASP) (plane wave basis) can't handle the localized charge in a system well due to the long range screening effect, all the calculation about the desolvation process are performed using Gaussian 03 package (atomic orbital basis) with HF/6-31+G*(d) basis.[6]

1.2 The adsorption process

The adsorption process for extracting M-ion from solvated M-ion in electrolytes into FePO4 surface is described as:

$$M^+(H_2O)_2\ (aq) + e^- + (FePO_4)_n(H_2O) \rightarrow M(FePO_4)_n(H_2O)_3 \qquad (4)$$

The reaction energy for Equation 4 is defined as:

$$\Delta G = G[M(FePO_4)_n(H_2O)_3]_{aq} - G[(FePO_4)_n(H_2O)]_{aq} - G[M^+(H_2O)_2]_{aq} - G[e^-] \qquad (5)$$

According to the work from Manna, et al,[7] the reaction energy can be further expressed as:

$$\Delta G = G[M(FePO_4)_n(H_2O)_3]_{aq} - G[(FePO_4)_n(H_2O)]_{aq} - G[M^+(H_2O)_2]_{aq} - EF \qquad (6)$$

Where E is the standard hydrogen potential, F is Faraday's constant. $M^+(H_2O)_2$ on the $FePO_4$ surface has the similar surrounding as the solvent M^+ in the electrolyte with the tails (…O–H) forming the hydrogen bonds with the solvent. As a result, we can use the reaction energy calculated in gas phase to be the approximate value for the reaction energy in liquid phase.

$\Delta G= G[M(FePO_4)_n(H_2O)_3]–G[(FePO_4)_n(H_2O)]–G[M^+(H_2O)_2]–EF$ (7)

Similarly, adsorption process of the solvated M-ion in EC can be described as:

$M^+(EC)(lq) + e^- + (FePO_4)_n \rightarrow Li(FePO_4)n(EC)$ (8)

We get the reaction energy as

$\Delta G = G[M(FePO_4)_n(EC)] – G[(FePO_4)_n] – G[M^+EC] – EF$ (9)

In the adsorption process, $G[FePO_4]$, $G[(FePO_4)_n(H_2O)]$, $G[M(FePO_4)_n(H_2O)_3]$ and $G[M(FePO_4)_n(EC)]$ are calculated with the VASP. The plane-wave projector-augmented wave method is used with an energy cut-off of 520 eV. The Perdew-Burke-Ernzerhof (PBE) form of the generalized gradient approximation (GGA) was chosen as the exchange-correlation potential. PBE+U approach is employed with the U value of 5.3 eV for Fe because of the strong on-site Coulomb interaction in the localized 3d electrons.[8] The $FePO_4$ (010) slab model is constructed from a 1×2×2 supercell and separated by a vacuum region of 12 Å.

$G[M^+(H_2O)_2]$ and $G[M^+EC]$are calculated using equations as follows:

$G[M^+(H_2O)_2]=G[M^+]+2G[(H_2O)]+ \Delta E_{2,\ 1\_H2O} +\Delta E_{1,1\_H2O}$ (10)

$G[M^+EC]= G[M^+]+G[EC]+\Delta E_{1,0\_EC}$ (11)

Where $G[(H_2O)]$ and $G[EC]$ are calculated using VASP with the molecular placed in the same supercell $FePO_4$ (010) to cancel the energy difference related to H_2O in equation 7 and EC in equation 9. Since VASP package can't well handle the ionic system, $G[M^+]$ is derived from the experimental Gibbs free energy for $M^+_{(aq)}$ from because the difference between the DFT results and the experimental ones is trivial.[9, 10]

Table S2 Successive detaching energies (eV) of the most stable structures of $Na^+(H_2O)_n$ (n = 1-6) and $Na^+(EC)_n$ (n = 1-4) in liquid phase based on HF/6-31+G*(d) method, with the corresponding energies for Li^+ in Ref.11 listed for comparison.

	EC		**H_2O**	
	Na^+	Li^+ [11]	Na^+	Li^+ [11]
$\Delta E_{6,5}$	--	--	0.25	--
$\Delta E_{5,4}$	--	--	0.26	--
$\Delta E_{4,3}$	0.41	0.01	0.46	0.51
$\Delta E_{3,2}$	0.71	0.42	0.62	0.80
$\Delta E_{2,1}$	1.15	1.29	0.79	1.14
$\Delta E_{1,0}$	1.46	1.81	0.89	1.32

Supporting section 2: Experimental details

Electrochemical driven ion-exchange process: $LiFePO_4$ powder was received from NanoChem Systems (Suzhou) without further treatment before use. The electrode film was fabricated using a mixture of $LiFePO_4$ powder (70 wt%), Vapor Grown Carbon Fiber (VGCF) (20 wt%), and polyvinylidene fluoride (10 wt%) in N-methylpyrrolidinon solution. The resulting slurry was cast onto Al foil using a doctor blade to have a loading level of around 3 mg cm^{-2} followed by dried first at 80 °C and then at 80 °C under a vacuum overnight. The electrochemical driven ion-exchange from $LiFePO_4$ to $NaFePO_4$ was carried out in a three-electrode break cell with a SCE and a Platinum piece as a reference and counter electrode, respectively. The electrolyte was composed of 0.5 M Li_2SO_4 or Na_2SO_4 (99.5%, Alfa Aesar) in distilled water. The $LiFePO_4$ electrode was cut into 5 x 4 cm pieces and galvanostatically delithiated to be $FePO_4$ at a 2.5 C rate (1 C=170 mA g^{-1}) to 0.55 V (*vs.* SCE) in Li_2SO_4 electrolyte; then the same electrode ($FePO_4$) was directly galvanostatically sodiated at 0.5C (1 C=170 mA g^{-1} based on the mass of $LiFePO_4$) to -0.9V (*vs.* SCE) in Na_2SO_4 electrolyte to be olivine $NaFePO_4$. The obtained $NaFePO_4$ electrode was washed by distilled water followed by dry at 80 °C under a vacuum overnight. For all the electrodes in the ion-exchange process the applied current and the resulting capacity were calculated from weight of the pristine $LiFePO_4$ electrode. Organic ion-exchange process was process following the reported classic process:[1] the $LiFePO_4$ electrode was galvanostatically delithiated at a 0.1 C rate (1 C=170 mA g^{-1}) to 4.2 V and then held at this voltage until the current reached a limit corresponding to a C/100 rate, this to assure the complete

$FePO_4$ formation process. The cell was then disassembled and the electrode washed using DMC (dimethyl carbonate) for three times in argon-filled glove box (soaked for at least 1 hr every time). The electrode was then transferred to a coin-type cell (R-2016) using a Na metal anode (Sigma-Aldrich) and a 1M $NaClO_4$ in a propylene carbonate (PC) / ethylene carbonate (EC) (1:1 in volume) electrolyte with 5% fluoro ethylene carbonate (FEC) (Tokyo Chemical Industry Co., Ltd) as electrolyte; and the electrochemical formation of the $NaFePO_4$ proceeded by galvanostatic reduction until 2.0 V *vs.* Na/Na^+ at a constant current of 0.1 C (1 C=154 mAg^{-1}).

Electrochemical measurement: The $NaFePO_4$ electrode was then assembled in a coin-type cell (R-2016) with pure sodium foil (Sigma-Aldrich) as the counter electrode, and a glass fibre as the separator in an argon-filled glove box (MBraun, Germany, O2 < 1ppm, H2O < 1ppm). The electrolyte is 1M $NaClO_4$ in a propylene carbonate (PC) / ethylene carbonate (EC) (1:1 in volume) electrolyte with 5% fluoro ethylene carbonate (FEC) (Tokyo Chemical Industry Co., Ltd) as additives. The charge and discharge measurements were carried out on a Land BT2000 battery test system in voltage ranges of 2-4V under room temperature. The hard carbon was received from Morgan AM&T Hairong Co., LTD. without further treatment. The mass balance between cathode and anode in full cell was fixed to 1:1.2. Due to large irreversible capacity, the anode was pre-active for one cycle in half-cell before assembled into full cell. All galvanostatic charge–discharge tests were carried out with on a Newware CT-3008W battery test system and BitrodeCorp. St. Louis Mo USA. Model: MCV 16-0.5/0.01-5 battery test station. Cyclic voltammetry and electrochemical impedance spectroscopy (EIS) were carried on cells using Autolab PGSTAT30 digital potentiostat/galvanostat at room temperature.

Materials Characterizations: Wide-angle X-ray diffraction (XRD) patterns were collected on Bruker D8 Focus Powder X-ray diffractometer using Cu Kα radiation (40 kV, 40 mA). Scanning electron microscopy (SEM) analysis was performed on JEOL-6701F SEM. Transmission electron microscopy (TEM) analysis was performed on an FEI Titan 80-300 S/TEM (Scanning /Transmission Electron Microscope) operated at 200 kV. The elemental maps were obtained by the three-window method using Gatan Image Filter (GIF). Ex-situ XRD experiments have been conducted. At different stages, electrodes were collected by disassembling the coin cells in Argon-filled glove box quickly. After rinsed in DMC (dimethyl carbonate), the electrodes were sealed in Kapton Tapes in Ar-filled glove box and sent to XRD characterization. Determination of metals (Li, Na, Fe) in solutions was conducted on Dual-view Optima 5300 DV ICP-OES system for identification and differentiation of elemental metals down to ppb levels.

Supporting references

1 S.-M. Oh, S.-T. Myung, J. Hassoun, B. Scrosati and Y.-K. Sun, *Electrochem. Commun.*, 2012, **22**, 149-152.
2 J. Mähler and I. Persson, *Inorganic Chemistry*, 2012, **51**, 425-438.
3 C. C. Pye, W. Rudolph and R. A. Poirier, *The Journal of Physical Chemistry*, 1996, **100**, 601-605.
4 X. Bogle, R. Vazquez, S. Greenbaum, A. v. W. Cresce and K. Xu, *J. Phys. Chem. Lett.*, 2013, **4**, 1664-1668.
5 S. Yanase and T. Oi, *Journal of Nuclear Science and Technology*, 2002, **39**, 1060-1064.
6 M. J. Frisch, *Gaussian 09*, Gaussian, Wallingford, CT, 2009
7 L. Manna, Wang, R. Cingolani and A. P. Alivisatos, *J. Phys. Chem. B*, 2005, **109**, 6183-6192.
8 F. Zhou, C. A. Marianetti, M. Cococcioni, D. Morgan and G. Ceder, *Phys. Rev. B*, 2004, **69**, 201101.
9 J. W. Johnson, E. H. Oelkers and H. C. Helgeson, *Computers & Geosciences*, 1992, **18**, 899-947.
10 K. A. Persson, B. Waldwick, P. Lazic and G. Ceder, *Phys. Rev. B*, 2012, **85**, 235438.
11 J. Zheng, Y. Hou, Y. Duan, X. Song, Y. Wei, T. Liu, J. Hu, H. Guo, Z. Zhuo, L. Liu, Z. Chang, X. Wang, D. Zherebetskyy, Y. Fang, Y. Lin, K. Xu, L.-W. Wang, Y. Wu and F. Pan, *Nano Lett.*, 2015, **15**, 6102-6109.